

# Present Status of the EMC effect <sup>1</sup>

Klaus Rith

Friedrich-Alexander-Universität Erlangen-Nürnberg  
 Physics Department  
 Erwin-Rommel-Str. 1  
 D-91058 Erlangen, Germany  
 E-mail: klaus.rith@physik.uni-erlangen.de

## Abstract

The present status of the EMC effect, the modification of the per nucleon cross section in deep-inelastic lepton nucleus scattering by the nuclear environment, is reviewed.

## 1 Introduction

The 30<sup>th</sup> anniversary of the publication by the European Muon Collaboration (EMC) [1] on the modification of the per-nucleon cross section of nucleons bound in nuclei, named *EMC effect*, is a good opportunity to review the status of the effect and to summarize the available experimental and theoretical information. The EMC effect can be interpreted as a modification of quark and gluon distributions in bound nucleons by the nuclear environment. The dependences of these nuclear modifications on kinematics and various nuclear properties like mass, density or radius are meanwhile rather well known, nevertheless the origin of the effect is still not fully understood. Recent data, discussed in section 6, provide new important input.

In my opinion further measurements of the effect in electron-nucleus, neutrino-nucleus and proton-nucleus scattering are needed to determine nuclear quark and gluon distributions (nPDFs) down to very low parton momentum fractions  $x$  and to constrain the initial state for the AA program at RHIC and LHC, or for the correct interpretation of, e.g., (future)  $\nu A$  experiments.

## 2 Deep-inelastic scattering, structure functions and quark distributions

Nuclear modifications of parton distributions have been studied mainly by measurements of cross sections in deep-inelastic lepton-nucleus scattering. For electromagnetic interactions of charged leptons with nuclear targets and in the approximation of one-photon exchange the cross section reads

$$\frac{d^2\sigma}{dQ^2dx} = \frac{4\pi\alpha^2}{Q^4} \frac{F_2(x, Q^2)}{x} \left[ 1 - y - \frac{Q^2}{4E^2} + \frac{y^2 + Q^2/E^2}{2[1 + R(x, Q^2)]} \right]. \quad (1)$$

---

<sup>1</sup>Lecture notes prepared for the Proceedings of the International School of Subnuclear Physics, Erice, 24 June – 3 July 2013

Here  $-Q^2$  represents the squared four-momentum of the virtual photon that mediates the interaction with coupling strength  $\alpha$  and  $x = Q^2/2M\nu$  can be interpreted as the fraction of the longitudinal nucleon momentum carried by the struck quark, in a frame where the nucleon moves with infinite momentum in the direction opposite to that of the virtual photon. The variable  $y$  denotes, in the target rest frame, the virtual-photon energy  $\nu$  with respect to the lepton-beam energy  $E$ .

At leading order in QCD the structure function  $F_2$  is defined as the sum of the momentum distributions  $q(x, Q^2)$  and  $\bar{q}(x, Q^2)$  of quarks and anti-quarks of flavor  $q = u, d, s, \dots$  weighted by  $x$  and  $z_q^2$ , where  $z_q$  is the quark charge (in units of the elementary charge  $|e|$ ):

$$F_2(x, Q^2) = \sum_{q=u,d,s,\dots} xz_q^2 [q(x, Q^2) + \bar{q}(x, Q^2)] . \quad (2)$$

The quantity

$$R = \frac{\sigma_L}{\sigma_T} = \frac{F_2}{2xF_1} \left[ 1 + \frac{4M^2x^2}{Q^2} \right] - 1 = \frac{F_L}{2xF_1} \quad (3)$$

is the ratio of the longitudinal to transverse virtual-photon cross sections. In the quark-parton model,  $R = 0$  for the interaction of the virtual photon with a point-like spin-1/2 particle. Quark transverse momenta, quark masses and gluon radiation cause  $R$  to deviate from zero. If  $R$  is independent of the nuclear mass number  $A$  (see the discussion in section 4.4), then the ratio of cross sections for two different nuclei is equal to the ratio of their structure functions  $F_2$ .

Subsequently, we will always discuss the ratio of structure functions (cross sections) per nucleon for a nucleus with mass number  $A$  (i.e.,  $A$  nucleons) and the deuteron  $D$ . The latter is, to a good approximation, equal to the proton-neutron averaged structure function  $F_2^D \approx (F_2^p + F_2^n)/2$ . The  $x$  dependence of the structure functions  $F_2^p$  and  $F_2^n$  is different (for free nucleons they are approximately related by  $F_2^n/F_2^p \approx 1 - 0.8x$ ). Results for the nuclear structure function  $F_2^A$  (cross section  $\sigma^A$ ) for nuclei with  $Z$  protons and  $N$  neutrons will always be corrected for neutron excess by

$$F_2^A = \left( \frac{F_2^p + F_2^n}{2} \right)^A \cdot \left[ 1 - \frac{N - Z}{N + Z} \cdot \frac{1 - F_2^n/F_2^p}{1 + F_2^n/F_2^p} \right] , \quad (4)$$

where it is assumed that proton and neutron structure functions are modified equally by the nuclear environment. Thus,  $F_2^A$  is the structure function per nucleon for a hypothetical isoscalar nucleus with an equal number ( $\frac{A}{2}$ ) of protons and neutrons.

### 3 The discovery

The historical result of the EMC effect [1] (updated results were published in [11]) is presented in the left panel of Fig. 1. It shows the ratio of the structure function  $F_2$  per nucleon for iron and deuterium, both uncorrected for Fermi motion, as a function of  $x$ . The shaded area indicates the range for the errors on the slope of a linear fit to the data, the point-to-point systematic uncertainties are somewhat larger. In addition there is an overall uncertainty of  $\pm 7\%$ .

The ratio is seen to be different from unity. It falls from  $\sim 1.15$  at  $x = 0.05$  to a value of  $\sim 0.89$  at  $x = 0.65$  and doesn't follow the expectations from Fermi-motion calculations. This

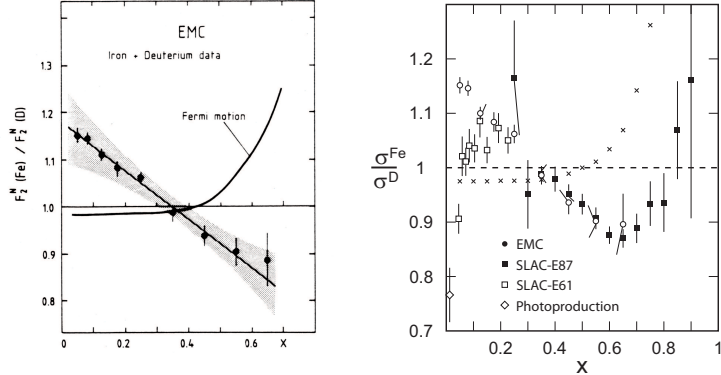


Figure 1: The ratio  $F_2^{\text{Fe}}/F_2^{\text{D}}$  ( $\sigma^{\text{Fe}}/\sigma^{\text{D}}$ ) as a function of  $x$ . Left panel: the original EMC result [1]; right panel: The SLAC result [3] together with low- $Q^2$  SLAC data for Cu/D [6] and the photoproduction result at  $Q^2 = 0$  GeV $^2$  [8]. Also shown is one expectation for the effect of Fermi motion on  $F_2^{\text{Fe}}$  in absence of other nuclear effects [5].

result demonstrated for the first time that the structure function  $F_2$  is modified when nucleons are embedded in a nucleus. At the time when these data were presented the effect appeared quite astounding. Especially members of the high-energy physics community could hardly believe that at momentum transfers several orders of magnitude larger than typical nuclear binding energies quark distributions should be affected by the nuclear environment. However, ‘quarks in nuclei’ and phenomena that could possibly modify the quark distributions in bound nucleons were already discussed by the nuclear-physics community for some time before this discovery. (For a first review of such ideas see Ref. [2]). The EMC result was quickly confirmed by the SLAC-MIT-Rochester group that recovered and reanalyzed the data stemming from the aluminum and steel cell walls of the liquid hydrogen and deuterium targets from the experiments E49B and E87. The result for  $\sigma^{\text{Fe}}/\sigma^{\text{D}}$  [3] is shown in the right panel of Fig. 1 together with earlier data from SLAC-E61 at lower  $Q^2$  for Cu/D in the range  $0.04 < x < 0.25$  [6] and a data point at  $Q^2 = 0$  GeV $^2$  from an experiment that had investigated shadowing in photoproduction [8]. (Similar data were published for aluminum [4]). At high  $x$ , these data were in good agreement with the EMC data, but the rather large value of  $F_2^{\text{Fe}}/F_2^{\text{D}}$  for the two low- $x$  EMC points was in disagreement with the low- $Q^2$  SLAC data which indicated that for  $x$  below  $\sim 0.15$  the ratio decreases again with decreasing  $x$ . (Indeed, it was found out later that the low- $x$  EMC points suffered from correlated tracking inefficiencies affecting the deuterium but not the iron data).

This exciting result caused enormous activities in both experiment and theory, resulting at present in about 1000 citations of the EMC publication [1]. The experimental data (with the exception of the recent JLAB data presented in Sect. 6) and many of the theory papers have been discussed in great detail some time ago in the excellent review by P. Norton [9]. Therefore, I will only summarize some of the key results and the main theoretical ideas for the interpretation of the effect.

## 4 The experimental data

After the discovery, nuclear effects have been studied experimentally in charged lepton-nucleus scattering by the muon experiments BCDMS [10], EMC-NA38 [12], EMC [13] and NMC [14, 15, 16, 17, 19, 20, 21] at CERN and E665 [22, 23] at FNAL, in electron scattering at SLAC [24, 25, 26, 27, 28], DESY [29] and JLAB [30, 31, 32, 33], in neutrino-nucleus scattering [34, 35] and in the Drell-Yan process [38, 39]. I will only discuss the most important results.

### 4.1 Data from SLAC-E139

At large  $x$  the most precise data are those from the SLAC experiment E139 [24] that measured the cross section ratio  $\sigma^A/\sigma^D$  for 8 nuclei ranging from  $^4\text{He}$  to  $^{197}\text{Au}$ . The results of an updated analysis with an improved treatment of radiative corrections [25] are shown in Fig. 2.

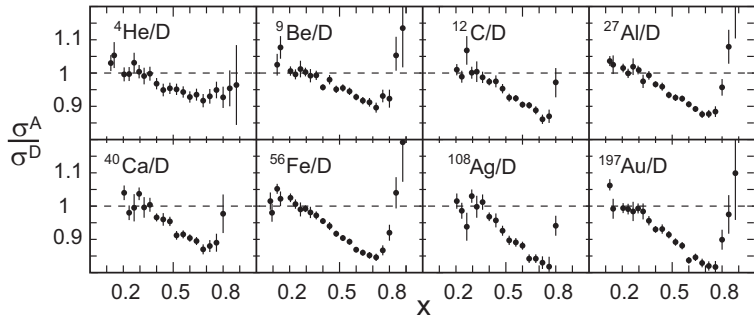


Figure 2: The ratio  $\sigma^A/\sigma^D$  as a function of  $x$  for various nuclei measured by SLAC-E139 [24, 25].

For all nuclei one observes, in the region  $0.3 < x < 0.8$ , a reduction of the per-nucleon cross section  $\sigma^A$  compared to the ‘free nucleon’ one,  $\sigma^D$ . The  $x$  dependence of this reduction has a very characteristic universal shape with a minimum near  $x \approx 0.7$ . The effect is already present for helium, its magnitude increases with the atomic mass number  $A$ . The  $A$  dependence will be discussed in more detail in section 4.8.

### 4.2 The universal $x$ dependence

The E139 data provide precise information for  $x > 0.2$ . The region of lower  $x$  is covered by the data from SLAC-E61[6], from the HERMES experiment [29], where the 27.6 GeV electron beam of HERA was scattered from internal gas targets of various nuclear species, and the muon experiments. As an example, the  $x$  dependence of the cross section ratio  $\sigma^{C(N)}/\sigma^D$  measured in electron scattering by E139 [25] and HERMES [29] is presented in Fig. 3. Also shown are data from JLAB-E03103 [32] taken with a beam energy of 5.8 GeV.

This figure nicely summarizes the universal  $x$  dependence of the nuclear effects. It can be subdivided into four  $x$  regions (plus a fifth one at  $x > 1$  which will be discussed separately in section 6):

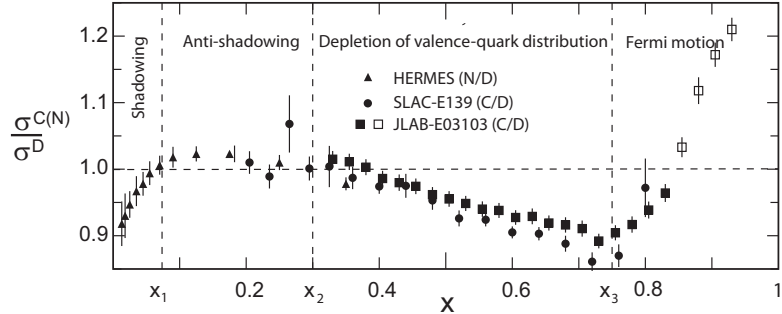


Figure 3: The ratio  $\sigma^{C(N)}/\sigma^D$  as a function of  $x$  from HERMES [29], SLAC-E139 [25], and JLAB-E03103 [32]. Open squares denote  $W^2$  below  $2 \text{ GeV}^2$ , where  $W$  is the invariant mass of the photon-nucleon system.

- the 'shadowing' region ( $0 < x < x_1 \simeq 0.06$ ), where the structure function ratio is smaller than unity and decreases with decreasing  $x$  down to the value measured in photoproduction. Here, the dominant contribution to the cross section is due to sea quarks. The essential longitudinal distances  $\Delta z$  probed in the deep-inelastic interaction (see section 5.1) are  $\Delta z > 3 \text{ fm}$ , much bigger than the size of a nucleon;
- the 'anti-shadowing' region ( $x_1 < x < x_2 \simeq 0.3$ ,  $3 \text{ fm} > \Delta z > 0.7 \text{ fm}$ ), where the ratio shows a small increase of a few percent over unity;
- the region ( $x_2 < x < x_3 \simeq 0.8$ ,  $\Delta z < 0.7 \text{ fm}$ ), where the ratio is smaller than unity with a minimum near  $x \approx 0.7$ . Here, the sea-quark distribution is essentially negligible and the ratio reflects the behavior of the valence-quark distributions;
- the region ( $x_3 < x < 1$ ), where the ratio increases rapidly with increasing  $x$ . This behavior is dominantly a kinematic effect since the free-nucleon cross section vanishes for  $x \rightarrow 1$ . It is partly also due to the Fermi motion of the bound nucleons in the nucleus.

### 4.3 Low- $x$ data

In deep-inelastic scattering from stationary targets, the kinematic region of very low  $x$  can only be accessed with muon beams, since those can be produced with much higher energies than electron beams. The first of such measurements was performed by EMC-NA28, using a muon detection system at small scattering angles down to 2 mrad and nuclear targets of C and Ca [12]. This experiment demonstrated that shadowing persist also at high values of  $Q^2$ . The low- $x$  region was then explored in detail by NMC with nominal incident muon energies of 90–200 GeV [14, 15, 16, 17, 19, 20, 21] and at even lower values of  $x$  by E665 at FNAL with a mean incident muon energy of 470 GeV.

NMC had the main objective to study the nuclear modification of the structure function  $F_2$  with high precision. Cross section ratios were measured for nine nuclear species. In one

set of measurements [14, 16, 18, 19]  ${}^4\text{He}$ ,  ${}^6\text{Li}$ ,  ${}^{12}\text{C}$  and  ${}^{40}\text{Ca}$  were compared to deuterium. All these nuclei are isoscalar and no correction for neutron excess (Equ. (4)) is necessary. In another set of measurements [20],  ${}^9\text{Be}$ ,  ${}^{27}\text{Al}$ ,  ${}^{40}\text{Ca}$ ,  ${}^{56}\text{Fe}$ ,  ${}^{119}\text{Sn}$  and  ${}^{207}\text{Pb}$  were compared to carbon. One important peculiarity of the NMC experiment was the multiple target arrangement. Targets of different materials were placed in a row at longitudinally well separated locations along the spectrometer axis and exposed simultaneously to the beam. Two such rows, differing in the ordering of materials, were placed on a common platform. The rows of targets were positioned in the beam in turn by lateral displacement of the platform at approximately 30–60 min intervals. With this arrangement beam flux and spectrometer acceptance corrections canceled in the determination of cross section ratios. These high-precision measurements are the low- $x$  counterpart of the E139 data at large  $x$ .

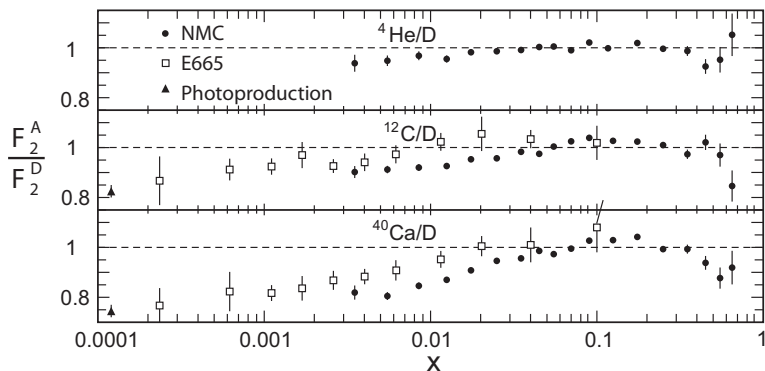


Figure 4: The ratio  $F_2^A/F_2^D$  for He, C and Ca measured at low  $x$  by NMC [19] and E665 [23]. Note that for both experiments  $Q^2 < 1 \text{ GeV}^2$  for  $x$  values below  $\approx 0.005$ .

As an example the structure function ratios of  ${}^4\text{He}$ ,  ${}^{12}\text{C}$  and  ${}^{40}\text{Ca}$  to deuterium measured by NMC [19] and E665 [23] are shown in Fig. 4. The E665 data nicely extrapolate to the shadowing results measured in photoproduction [8]. The NMC and E665 data do not agree very well, but the E665 data move downwards by a few percent, when another method of radiative corrections is applied [23]. As already seen in Fig. 3, the ratio is smaller than unity below  $x_1 \approx 0.06$  and decreases with decreasing  $x$ . The effect is already visible for  ${}^4\text{He}$ , it increases with  $A$ .

#### 4.4 Nuclear dependence of $\mathbf{R}$

As stated in section 2,  $\sigma^A/\sigma^D$  is only equal to  $F_2^A/F_2^D$ , if the quantity  $\mathbf{R}$  is independent of the nuclear mass number  $A$ . The nuclear dependence of  $\mathbf{R}$  has been studied by SLAC-E140 [26, 27], NMC [15, 21] and HERMES [29]. All measurements are consistent with  $\mathbf{R}$  being independent of  $A$ . A reanalysis of all SLAC data with an improved radiative-corrections calculation procedure [27] resulted in  $R^{\text{Fe}} - R^D = 0.001 \pm 0.018(\text{stat.}) \pm 0.016(\text{sys.})$ , and the authors conclude that possible contributions to  $\mathbf{R}$  from nuclear higher-twist effects and possible spin-0 constituents in nuclei

are not different from those in free nucleons. This conclusion is supported by the more recent HERMES measurement [29]. Averaging over all measurements of  $R^A/R^D$  for light and medium heavy nuclei ( $^3\text{He}$ ,  $^4\text{He}$ ,  $^{12}\text{C}$ ,  $^{14}\text{N}$ ) HERMES obtained an average value for  $R^A/R^D$  of  $0.99 \pm 0.03$ . The result is unchanged if also the data on the heavier nuclei are included in the average.

#### 4.5 $Q^2$ dependence of the nuclear effects

Already from the good agreement between the muon and the electron data one can conclude that the  $Q^2$  dependence of the nuclear effects is very small, since, at the same value of  $x$ , their average  $Q^2$  typically differs by more than an order of magnitude.

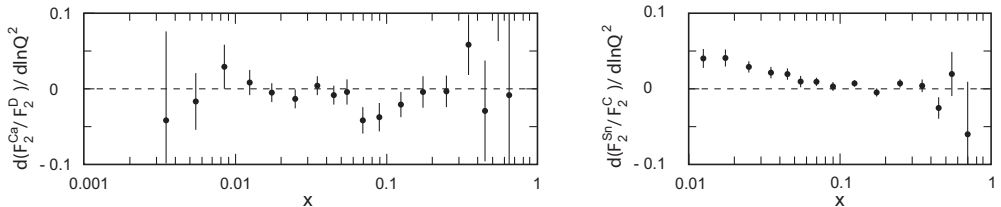


Figure 5: NMC results for the  $x$  dependence of the logarithmic slope  $d(F_2^A/F_2^D)/d\ln Q^2$ . Left panel: Ca/D [19], right panel: Sn/C [21].

The  $Q^2$  dependence was studied in some detail by NMC [18, 21], FNAL-E665 [23] and HERMES [29]. As an example, the left panel of Fig. 5 shows the  $x$  dependence of the logarithmic slope  $d(F_2^{\text{Ca}}/F_2^{\text{D}})/d\ln Q^2$  from fits of the form  $F_2^A/F_2^D = a + b \cdot \ln Q^2$  to the NMC data [19]. In the covered  $Q^2$  range there is little indication for a  $Q^2$  dependence of the ratio. The NMC Sn/C data [21], shown in the right panel of Fig. 5, are the only exception where one observes an indication of a small  $Q^2$  dependence at small values of  $x$ .

#### 4.6 Neutrino data

The available measurements in neutrino/antineutrino-nucleus scattering [34, 35] suffer from their large statistical and systematic uncertainties and do not provide additional information. Apart from [34] all these measurements have been performed with bubble chambers. Precise measurements of neutrino and antineutrino scattering from deuterium and heavy nuclear targets would be very helpful for a separation of nuclear effects in sea-quark and valence-quark distributions and a determination of nuclear parton distribution functions (nPDFs). But such measurements have to wait for the future realization of a very-high-luminosity neutrino factory.

#### 4.7 Drell-Yan data

The nuclear modification of anti-quark distributions can also be investigated by the Drell-Yan process [37] in proton-nucleus scattering:  $pA \rightarrow (l + l^-)X$ . In this process a quark (anti-quark) with the four-momentum fraction  $x_1$  from the beam proton and an anti-quark (quark) of the

target nucleon with  $x_2$  annihilate electromagnetically into a virtual photon, which immediately decays into a charged-lepton pair:  $q(x_1)\bar{q}(x_2) \rightarrow \gamma^* \rightarrow l^+l^-$ .

The longitudinal momentum of the  $l^+l^-$  pair in the proton-nucleon center-of-mass system is approximately given by  $p_L^{l^+l^-} \approx (x_1 - x_2)\sqrt{s}/2$  and its invariant mass by  $(M_{l^+l^-})^2 = x_1 x_2 s$ . Here,  $\sqrt{s}$  is the nucleon-nucleon center-of-mass energy. The Drell-Yan cross section reads

$$\frac{d^2\sigma}{dx_1 dx_2} = K \frac{4\pi\alpha^2}{9x_1 x_2} \frac{1}{s} \sum_{q=u,d,s,\dots} z_q^2 [q(x_1)\bar{q}(x_2) + \bar{q}(x_1)q(x_2)], \quad (5)$$

where  $K \approx 2$  is a factor representing the deviation from the simple parton model due to QCD corrections. By a suitable choice of the kinematics of the  $l^+l^-$  pair the quark and anti-quark distributions in the target can be determined separately. If one requires for instance  $x_1 - x_2 > 0.3$ , then the second term in (5) can be neglected and the cross section ratio for two nuclei  $A_1$  and  $A_2$  is to a good approximation equal to the ratio of anti-quark distributions  $\bar{q}^{A_1}/\bar{q}^{A_2}$  in the target.

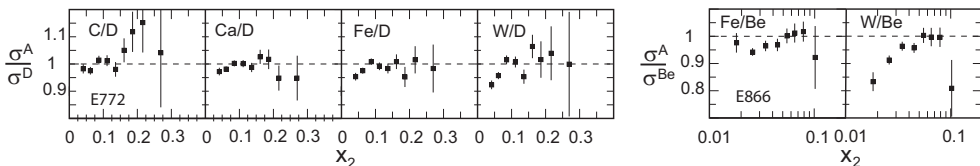


Figure 6: Drell-Yan results for the cross-section ratio  $\sigma^A/\sigma^D$  [38] (left) and  $\sigma^A/\sigma^{Be}$  [39] (right) as a function of  $x_2$ .

In the left panel of Fig. 6,  $\sigma^A/\sigma^D$  for four nuclei (C, Ca, Fe, W) measured by FNAL-E772 [38] is shown as a function of  $x_2$ , whereas the right panel shows  $\sigma^A/\sigma^{Be}$  for (Fe, W) measured by FNAL-E866 [39], both with a proton-beam energy of 800 GeV. At the smallest  $x_2$  values the data show an indication of shadowing, while above  $x_2 \approx 0.06$  the ratios are consistent with unity (with the exception of the C/D data) leading to the conclusion that anti-shadowing is very likely not a sea-quark effect or caused by nuclear pions. This aspect will be studied in detail by the experiment E906/Seaquest at the 120 GeV beam of the FNAL Main Injector [40].

Unfortunately the Drell-Yan cross section is very small and it is very difficult to study the process with colliding ion beams at much higher center-of-mass energies. Nevertheless such measurements in proton-deuteron and proton-nucleus collisions at RHIC or the LHC would be very desirable for the determination of nPDFs at low values of  $x$ .

#### 4.8 Dependence on nuclear properties

**Dependence on nuclear mass A.** From Figs. 2 and 4 it is obvious that the nuclear effects increase continuously with nuclear mass number A. This aspect has been studied in detail by E139 [25] and NMC [20].

The left panel of Fig. 7 shows the NMC results [20] for the dependence of  $F_2^A/F_2^C$  on A for the two bins  $x = 0.0125$  and  $x = 0.175$ , and the upper plot in the right panel shows the E139

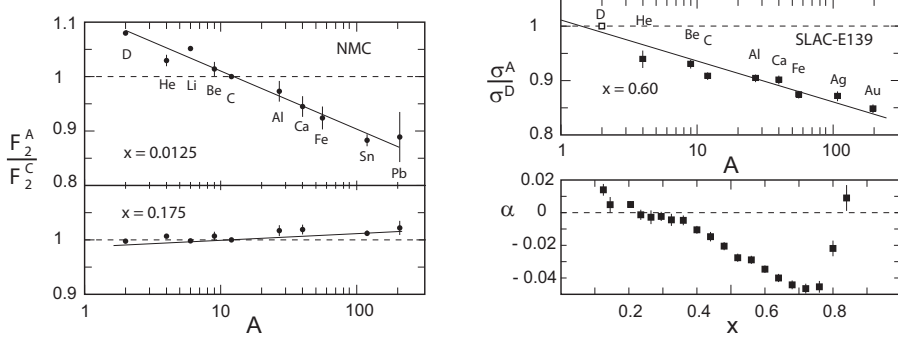


Figure 7:  $F_2^A/F_2^C$  as a function of nuclear mass  $A$  at low  $x$  from NMC [20] (left) and  $\sigma^A/\sigma^D$  at high  $x$  from SLAC-E139 [25] (right). The lower right panel shows the coefficient  $\alpha(x)$  from a fit of the form  $\sigma^A/\sigma^D(x) = c(x)A^{\alpha(x)}$ .

results [25] for  $\sigma^A/\sigma^D$  in the bin  $x = 0.60$ . Obviously the nuclear effects increase to a good approximation linearly with  $\log A$ . Small deviations from this linear dependence are observed in the left panel for He and Li and in the right panel for He and C. Obviously there are other nuclear properties than  $A$  affecting the nuclear dependence. The lines are results of fits of the form: Ratio =  $c(x)A^{\alpha(x)}$ . The coefficient  $\alpha(x)$  determined from the E139 data is shown in the lower right panel as a function of  $x$ . If we rewrite  $\alpha(x)$  as  $\alpha(x) = \alpha'(x) - 1$ , then  $A^{\alpha'(x)}$  can be interpreted as the effective number of nucleons participating in the interaction.

**Dependence on nuclear density  $\rho$ .** One important aspect for the understanding of the nuclear medium effects is their dependence on the nuclear density  $\rho$ . In Fig. 8 the data presented in Fig. 7 are shown as a function of  $\rho$  in four bins of  $x$ .

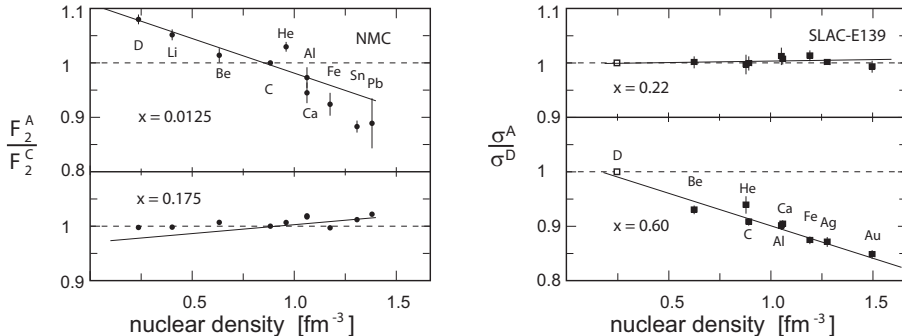


Figure 8:  $F_2^A/F_2^C$  as a function of nuclear density  $\rho$  at low  $x$  from NMC [20] and  $\sigma^A/\sigma^D$  at high  $x$  from SLAC-E139 [25].

Here  $\rho(A)$  is given by  $\rho(A) = 3A/4\pi R_e^3$ , with  $R_e^2 = 5 < r^2 > /3$ , and  $< r^2 >$  is taken from Ref. [41]. At large  $x$  the cross section ratio approximately scales with  $\rho$ , with the exception of the rather special nuclei  $^4\text{He}$  and  $^9\text{Be}$ . The deviation of  $^9\text{Be}$  from this linear behavior is, however, much smaller than in the analysis of JLAB-E03103 [32], where a density based on ab initio few-body calculations [42], scaled by  $(A - 1)/A$  is used. The small- $x$  data are not well described by a linear function of nuclear density.

**Dependence on nuclear radius  $r$ .** The deviations from a linear behavior observed in Fig. 8 indicate that besides the nuclear density other parameters like the nuclear radius or the nuclear surface may play a role. The nuclei  $^4\text{He}$ ,  $^6\text{Li}$ ,  $^{12}\text{C}$  and  $^{40}\text{Ca}$  have been used by NMC [14, 15, 18, 19] to possibly differentiate between effects originating from the nuclear density or from the nuclear radius. These nuclei differ primarily either in radius ( $r$ ) or density ( $\rho$ ). In particular,  $^6\text{Li}$  ( $r = 2.6$  fm,  $\rho = 0.04$  fm $^{-3}$ ) and  $^{12}\text{C}$  ( $r = 2.5$  fm,  $\rho = 0.09$  fm $^{-3}$ ) have nearly equal radii but different densities, whereas  $^4\text{He}$  ( $r = 1.7$  fm,  $\rho = 0.09$  fm $^{-3}$ ) and  $^{12}\text{C}$  have nearly equal densities but different radii.  $^{12}\text{C}$  and  $^{40}\text{Ca}$  ( $r = 3.5$  fm,  $\rho = 0.11$  fm $^{-3}$ ) differ more in radius than in density. The analysis presented in [15] demonstrates that there is a rather complicated interplay between the dependences on radius and density: the depletion at low  $x$  is larger in  $^{12}\text{C}$  than in  $^6\text{Li}$ , showing that at the same radius the effect increases with  $\rho$ ; the comparison of the pairs ( $^4\text{He}, ^{12}\text{C}$ ) and ( $^{40}\text{Ca}, ^{12}\text{C}$ ) indicates that at similar densities the effect increases with radius; the depletion in  $^{40}\text{Ca}$  is twice as large than in  $^6\text{Li}$ , implying that the depletion increases with both radius and density; and the Li/He ratio is consistent with unity over the common  $x$  range, indicating that the opposing dependencies on radius and density tend to cancel. Furthermore NMC has shown that at low  $x$  the data are best described by a fit of the form  $F_2^A/F_2^C = a + bA^{-1/3} + cA^{-2/3}$  [20].

## 5 Interpretations

It is beyond the scope of this lecture note to address the multitude of possible explanations for the observed nuclear medium effects (for a rather detailed discussion see Ref. [9]). Instead, only the main ideas of some classes of models will be summarized without a discussion why and where they fail to reproduce the data correctly.

### 5.1 Shadowing

The first class of models deals with the shadowing region. The term ‘shadowing’ has been introduced to explain the reduction of the nuclear cross sections in photoproduction, but has then also been used in the discussion of the low- $x$  modification of the nuclear cross section in inelastic lepton-nucleon scattering. There are two possibilities to explain this phenomenon. In the first approach the parton distributions in bound nucleons remain unchanged compared to those in the free nucleon. The interaction is viewed in the rest system of the nucleus. The nuclear effects are attributed to a modification of the interaction of the virtual photon with the atomic nucleus by fluctuations of the virtual photon into quark-antiquark pairs. Such a pair then interacts with the nucleus via the *strong* interaction. Since the strength of the latter is much larger than the electromagnetic one, the interaction does no longer happen incoherently with all

the nucleons in the nucleus but preferentially with those at the front surface. The nucleons being in the ‘shadow’ of the nucleons at the front surface then do not or much less contribute to the cross section. Quantitatively this happens, when the fluctuation length  $\Delta d \approx 1/Mx \approx 0.2 \text{ fm}/x$  is larger than the mean free path  $L \cong 2.5 \text{ fm}$  of the quark-antiquark pair, i.e., for  $x$  below  $\approx 0.08$ .

In the second approach the effect is attributed to a modification of the quark and gluon distributions in the nucleus. The interaction of the virtual photon with the nucleus is viewed in a fast moving system, where the nucleon with diameter  $D$  is Lorentz contracted to a disc of thickness  $D' \approx D \cdot M/|\vec{P}|$  and the mean nucleon distance  $d \approx 2 \text{ fm}$  to  $d' = d \cdot M/|\vec{P}|$ . The longitudinal position of its constituents, however, has an uncertainty of  $\Delta z = 1/x|\vec{P}|$ . At small values of  $x$  this uncertainty  $\Delta z$  can be much larger than  $D'$  and in a nucleus much larger than  $d'$ . For  $x < 1/d \cdot 1/M \approx 0.1$  there will be a spatial overlap of sea quarks and gluons of different nucleons. The smaller  $x$ , the larger is the number of nucleons sharing their contents of sea-quarks and gluons. The effect increases with increasing mass number  $A$  and saturates for  $x \approx 1/D_A \cdot 1/M$ , where  $D_A$  is the diameter of the nucleus in its rest frame. Thus, the density of gluons and sea quarks at the position of a nucleon in a nucleus can be much larger than for a free nucleon. Due to this ‘overcrowding’ the probability for an interaction between sea quarks and gluons is increased and by pair annihilation their density is reduced again, resulting in the observed reduction of the nuclear structure function. Momentum conservation requires that this reduction of the number of partons at low values of  $x$  gets compensated by an enhancement at larger  $x$ , i. e., anti-shadowing.

Both approaches for shadowing are equivalent. They describe the same phenomenon but viewed in a different reference frame. More details can be found, e. g., in Refs. [43, 44].

## 5.2 Convolution Models

In the second class of models the structure function of a nucleus  $A$  is described as the incoherent sum over contributions of all kind of clusters  $c$  with structure functions  $F_2^c(x/y)$  convoluted with the probability  $f_c^A(y)$  to find a certain cluster  $c$  of momentum  $y$  in the nucleus:

$$F_2^A(x, Q^2) = \sum_c \int_x^A dy f_c^A(y) F_2^c(x/y). \quad (6)$$

Examples for such clusters are the nucleon itself, undisturbed or with a reduced mass due to nuclear binding or with an increased size due to different boundary conditions in the nuclear environment, extra pions being responsible for nuclear binding,  $\Delta$ -isobars, multi-quark clusters like bags of 6 quarks, 9 quarks or 12 quarks (i.e.,  $\alpha$  particles) or the whole nucleus as one big bag with free quark and color flow throughout the whole nuclear volume.

There is a lot of freedom in these approaches, concerning as well the choice of  $f_c^A(y)$  as the parameterization of  $F_2^c(x/y)$  that both are badly known. Consequently, it is not very surprising that they succeed to reproduce a portion of the data rather well, at least in the medium  $x$  range.

### 5.3 Rescaling models

In the third class of approaches the EMC effect is explained by a change of either the  $Q^2$  scale or the  $x$  scale for the nuclear structure function compared to the free nucleon's one.

**$Q^2$  rescaling.** In  $Q^2$  rescaling models, first proposed in Refs. [45] and [46], the EMC effect is related to a change of confinement size inside the nucleus. The  $A$  dependence of quark and gluon distributions for bound nucleons and the  $Q^2$  evolution of these distributions for free nucleons both have the same origin. They are caused by the color forces between quarks and gluons which ensure confinement and are the origin of scaling violations, i.e., the increase of the structure function with  $Q^2$  at low values of  $x$  and the decrease with increasing  $Q^2$  at large values of  $x$ . The qualitative argument is as follows: The strength of the strong force between quarks is not only determined by the transverse resolution  $1/\sqrt{Q^2}$  at which they are probed, but also by the radial extension  $r_A$  of the volume in which they are confined. Therefore, the relevant parameter for the strength of the strong coupling constant  $\alpha_s$  is not just  $Q^2$  but  $(Q \cdot r_A)^2$ . (This is similar to the situation in nuclear physics where the form factors for spherical nuclei have the identical oscillating pattern when plotted against  $(Q \cdot r_A)$ ). If the confinement size is modified inside the nucleus, either due to a 'swelling' of nucleons, the formation of multi-quark bags, short-range nucleon-nucleon correlations or free quark and color flow throughout the whole nucleus, then, as a consequence, quark and gluon distributions obtained for nuclei  $A$  and  $B$  are related by

$$q_A(x, Q^2) = q_B(x, \xi \cdot Q^2), \quad g_A(x, Q^2) = g_B(x, \xi \cdot Q^2). \quad (7)$$

$\xi$  is a rescaling parameter determined by the two confinement scales  $r_A$  and  $r_B$ . In the so-called 'dynamical rescaling' models it is given by

$$\xi = (r_A/r_B)^{2\alpha_s(\mu_A^2)/\alpha_s(Q^2)}, \quad (8)$$

where  $\mu_A$  is a low-momentum cut-off for radiating gluons. Consequently, at the same value of  $Q^2$ ,  $F_2^A/F_2^B > 1$  for small values of  $x$  and  $F_2^A/F_2^B < 1$  for large values of  $x$ , if  $r_A > r_B$ .

**$x$  rescaling.** In the  $x$ -rescaling models, first proposed in [47, 48] and then refined by numerous authors, the depletion of the nuclear structure function at medium  $x$  is explained by conventional nuclear binding and Fermi-motion corrections. The  $x$  dependence can be reasonably well reproduced if, for a nucleus, the scaling variable  $x$  is replaced by a modified one  $x^* > x$ . For a nucleon  $i$  moving with momentum  $\vec{p}_i$  in a nucleus the variable  $x = Q^2/2M\nu$  has to be replaced by

$$x_i = Q^2/2p_i q = Q^2 / [2(M + E_i)\nu - 2\vec{p}_i \vec{q}], \quad (9)$$

where  $E_i$  is the removal energy of the nucleon ( $\langle E_i \rangle \cong -25$  MeV) and  $\vec{q}$  is the momentum of the virtual photon. Consequently, at the same kinematics of the scattered lepton, the effective  $x^*$  at which the structure function is probed in a nucleus, is larger than  $x$  for a free nucleon. At large  $x$  the structure function  $F_2$  is steeply falling with  $x$  and a depletion of the structure function ratios is naturally explained.

## 6 The new ingredient: $x > 1$

Recently there has been renewed interest in the EMC effect and its possible origin by JLAB measurements of the cross section ratios in inclusive electron scattering  $A(e, e')$  in the kinematic region  $x > 1$  where the cross section vanishes for scattering from free nucleons.

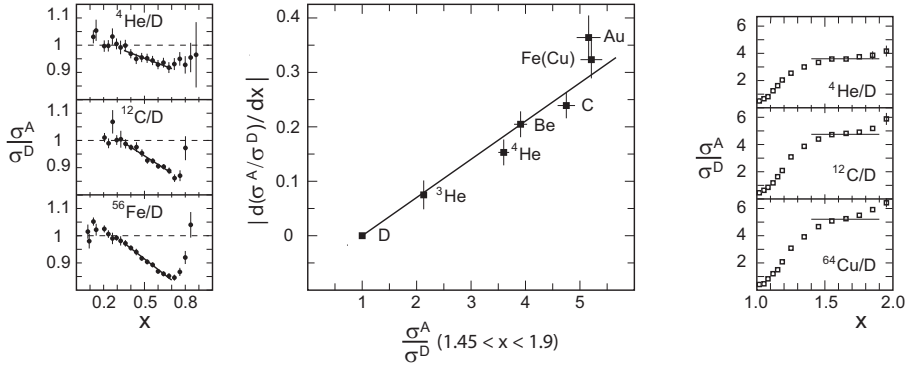


Figure 9: The cross section ratio  $\sigma^A/\sigma^D$  measured by SLAC-E139 at  $x < 1$  (left panel) and by JLAB-E02019 in the region  $1 < x < 2$  (right panel). The middle panel shows the correlation between the slope  $|d(\sigma^A/\sigma^D)/dx|$  in the region  $0.35 \leq x \leq 0.7$  and the height of the plateau of  $\sigma_A/\sigma_D$  in the region  $1.45 < x < 1.9$  (after [36]).

The CLAS experiment [30, 31] has measured  $\sigma^A/\sigma^{{}^3\text{He}}$  for  ${}^4\text{He}$ ,  ${}^{12}\text{C}$  and  ${}^{56}\text{Fe}$  and JLAB-E02019 [33] measured  $\sigma^A/\sigma^D$  for  ${}^3\text{He}$ ,  ${}^4\text{He}$ , Be, C, Cu and Au. In the right panel of Fig. 9 the cross section ratios  ${}^4\text{He}/\text{D}$ ,  $\text{C}/\text{D}$  and  $\text{Cu}/\text{D}$  are shown as a function of  $x$ . They rise with  $x$  until they reach a plateau at  $x \approx 1.4 - 1.5$ . The height of this plateau increases with  $A$ . Such a behavior has already been observed with less accuracy by an experiment at SLAC [28]. A similar pattern is seen in the CLAS comparison of the nuclear cross sections to  ${}^3\text{He}$ . Here the measurements extend up to  $x = 3$  and an indication of a second plateau is observed for  $x > 2.25$ . Such a behavior is being interpreted as the manifestation of short-range nucleon-nucleon (mostly p-n) correlations (three-nucleon correlations for  $x$  beyond 2) or, in another approach, as the ratio of the probabilities to find 6-quark or 9-quark clusters in nuclei compared to the reference nucleus.

Fig. 9 shows a very interesting observation [36]. In the left panel the E139 cross section ratios  ${}^4\text{He}/\text{D}$ ,  $\text{C}/\text{D}$  and  $\text{Fe}/\text{D}$  are shown for  $x < 1$ . The lines correspond to the slopes  $d(\sigma^A/\sigma^D)/dx$  in the region  $0.35 \leq x \leq 0.7$ , that characterize the strength of the EMC effect in this region and are unaffected by overall normalization uncertainties. In the middle panel the slopes of the E139 data (tabulated in [36] and corrected by  $x_A = x_p \cdot A M_p / M_A$  [49]) are plotted against the height of the plateaus [33]. Obviously there is a strong correlation between these quantities as indicated by the straight line. It is rather unlikely that this correlation is purely accidental and one can therefore rather safely assume that a large fraction of the strength of the EMC effect in the valence quark region is due to short-range nucleon-nucleon correlations.

## 7 Summary and Outlook

The EMC effect is with us now for 30 years. It has stimulated huge experimental and theoretical efforts, but its origin is still not fully understood. Recent data shed some new light on its possible origin, i.e., short-range nucleon-nucleon correlations may play an important role for the observed nuclear modifications. Still more precise data are needed, especially on the nuclear gluon and antiquark distributions at very low  $x$  to constrain the initial state for the AA program at RHIC and LHC. These hopefully will come from future measurements at JLAB12, RHIC and LHC and eventually also from the proposed projects EIC and LHeC.

## References

- [1] J. J. Aubert et al. (EMC), Phys. Lett. **B 123** (1983) 275.
- [2] K. Rith, Proceedings of the Eighteenth Rencontre de Moriond, Vol. 2, J. Tran Thanh Van ed., Editions Frontieres, 1983, pp. 207-222.
- [3] A. Bodek et al. (SLAC), Phys. Rev. Lett. **50** (1983) 1431.
- [4] A. Bodek et al. (SLAC), Phys. Rev. Lett. **51** (1983) 534.
- [5] A. Bodek and J. L. Ritchie, Phys. Rev. **D 23** (1981) 1070; **D 24** (1981) 1400.
- [6] S. Stein et al. (SLAC), Phys. Rev. **D 12** (1975) 1884.
- [7] S. Rock and P. Bosted, Phys. Lett. **B 518** (2001) 34.
- [8] D. O. Caldwell et al., Phys. Rev. Lett. **42** (1979) 553.
- [9] P. R. Norton, Rept. Prog. Phys. **66** (2003) 1253.
- [10] G. Bari et al. (BCDMS), Phys. Lett. **B 163** (1985) 282; A. C. Benvenuti et al. (BCDMS), Phys. Lett. **B 189** (1987) 483.
- [11] J. J. Aubert et al. (EMC), Nucl. Phys. **B 293** (1987) 740.
- [12] M. Arneodo et al. (EMC-NA38), Phys. Lett. **B 211** (1988) 493; Nucl. Phys. **B 333** (1990) 1.
- [13] J. Ashman et al. (EMC), Phys. Lett. **B 202** (1988) 603; Z. Phys. **C 57** (1993) 211.
- [14] P. Amaudruz et al. (NMC), Z. Phys. **C 51** (1991) 387.
- [15] P. Amaudruz et al. (NMC), Phys. Lett. **B 294** (1992) 120.
- [16] P. Amaudruz et al. (NMC), Z. Phys. **C 53** (1992) 73.
- [17] P. Amaudruz et al. (NMC), Nucl. Phys. **B 371** (1992) 553.
- [18] P. Amaudruz et al. (NMC), Nucl. Phys. **B 441** (1995) 3.
- [19] M. Arneodo et al. (NMC), Nucl. Phys. **B 441** (1995) 12.
- [20] M. Arneodo et al. (NMC), Nucl. Phys. **B 481** (1996) 3.
- [21] M. Arneodo et al. (NMC), Nucl. Phys. **B 481** (1996) 23.

[22] M. R. Adams et al. (FNAL-E665), Phys. Rev. Lett. **68** (1992) 3266; Phys. Lett. **B 287** (1992) 375.

[23] M. R. Adams et al. (FNAL-E665), Z. Phys. **C 67** (1995) 403.

[24] R. G. Arnold et al. (SLAC-E139), Phys. Rev. Lett. **52** (1984) 727.

[25] J. Gomez et al. (SLAC-E139), Phys. Rev. **D 49** (1994) 4348.

[26] S. Dasu et al. (SLAC-E140), Phys. Rev. Lett. **60** (1988) 2591.

[27] S. Dasu et al. (SLAC-E140), Phys. Rev. **D 49** (1994) 5641.

[28] L. Frankfurt et al., Phys. Rev. **C 48** (1993) 2451.

[29] A. Airapetian et al. (HERMES), Phys. Lett. **B 567** (2003) 339.

[30] K. Egyan et al. (JLAB-CLAS), Phys. Rev. **C 68** (2003) 014313.

[31] K. Egyan et al. (JLAB-CLAS), Phys. Rev. Lett. **96** (2006) 082501.

[32] J. Seely et al. (JLAB-E03103), Phys. Rev. Lett. **103** (2009) 202301.

[33] N. Fomin et al. (JLAB-E02019), Phys. Rev. Lett. **108** (2012) 092502.

[34] H. Abramowicz et al. (CDHS), Z. Phys. **C 25** (1984) 29.

[35] A. M. Cooper et al., Phys. Lett. **B 141** (1984) 133; M. A. Parker et al., Nucl. Phys. **B 232** (1984) 1; V. V. Ammosov et al., JETP Lett. **39** (1984) 393; J. Hanlon et al., Phys. Rev. **D 32** (1985) 2441; A. E. Asratyan et al., Sov. J. Nucl. Phys. **41** (1985) 763; Sov. J. Nucl. Phys. **43** (1986) 380; M. Aderholz et al., Phys. Lett. **B 173** (1986) 211; J. Guy et al., Z. Phys. **C 36** (1987) 337; J. Guy et al. , Phys. Lett. **B 229** (1989) 421; T. Kitagaki et al., Phys. Lett. **B 214** (1988) 281.

[36] L. B. Weinstein et al., Phys. Rev. Lett. **106** (2011) 052301.

[37] S. Drell and T.-M. Yan, Phys. Rev. Lett. **25** (1970) 316; Erratum-ibid. **25** (1970) 902.

[38] D. M. Alde et al. (FNAL-E772), Phys. Rev. Lett. **64** (1990) 2479.

[39] M. A. Vasiliev et al. (FNAL-E866), Phys. Rev. Lett. **83** (1999) 2304.

[40] P. Reimer, Proceedings of Spin 2010, Jülich, Germany; J. Phys.: Conf. Ser. **295** (2011) 012011.

[41] H. De Vries et al., Atomic Data and Nuclear Tables **36** (1987) 495.

[42] S. C. Pieper and R. B. Wiringa, Ann. Rev. Nucl. Part. Sci. **51** (2001) 53.

[43] B. Z. Kopeliovich, J. Morfin and I. Schmidt, Prog. Part. Nucl. Phys. **68** (2013) 314.

[44] L. Frankfurt, V. Guzey and M. Strikman, Phys. Rept. **512** (2012) 255.

[45] F. E. Close et al., Phys. Lett. **B 129** (1983) 346.

[46] O. Nachtmann and H. J. Pirner, Z. Phys. **B 21** (1984) 277.

[47] C. H. Garcia Canal et al., Phys. Rev. Lett. **53** (1984) 1430.

[48] M. Staszek et al., Phys. Rev. **D 29** (1984) 2638.

[49] L. Frankfurt and M. Strikman, Int. J. Mod. Phys. **E 21** (2012) 1230002.